Comparison of Bistatic Clutter Mitigation Algorithms For Varying Geometries

William L. Melvin, Ph.D., Georgia Tech Research Institute
Michael J. Callahan, Air Force Research Laboratory
Mark E. Davis, Ph.D., Air Force Research Laboratory

Key Words: Space-time adaptive processing (STAP), bistatic radar

Abstract – Airborne bistatic radar systems require effective techniques to mitigate the impact of ground clutter returns on detection performance. Bistatic clutter generally appears more severe than in monostatic systems owing to increased two-way antenna gain over a broad set of angles and greater clutter spectral variation over range. Adaptive filtering seems like a natural response to combat both of these effects. However, the consequent clutter non-stationarity – variation of clutter angle-Doppler response with range – presents difficulty when implementing the adaptive filter, since such an effect leads to errors in the requisite clutter covariance matrix estimate. Approaches for coping with clutter non-stationarity are central to effective bistatic space-time adaptive processing (STAP) techniques. In this paper we consider the impact of sensor geometry on the performance of several recently proposed bistatic STAP techniques. Our findings suggest best performance for those methods providing pre-STAP compensation of the data in both angle and Doppler.

1. *INTRODUCTION*

Bistatic radar systems offer several advantages over their monostatic counterparts, including reduced space loss, silent operation, reduced susceptibility to jamming, and synergistic coherent operation with existing systems. Among the drawbacks, bistatic aerospace radar systems must effectively cope with severe, spectrally diverse ground clutter returns. For this reason, effective bistatic clutter cancellation techniques are crucial for air-to-surface bistatic radar system deployment.

The classes of adaptive clutter filtering techniques developed for monostatic airborne radar – *viz.*, space-time adaptive processing (STAP) and its variants [1-6] – offer a logical starting framework in the bistatic case. However, the non-stationary nature of bistatic ground clutter directly violates intrinsic adaptive algorithm assumptions, thereby complicating STAP implementation, and potentially degrading detection performance [4, 7-8]. In response to this challenge, a variety of non-stationary clutter mitigation techniques have been recently proposed [9-17]. These various methods exhibit differing performance, depending on the scenarios presented. The purpose of this paper is to consider the impact of sensor geometries on the class of bistatic, data warping STAP techniques [11,13,14,15,17]. We illustrate the performance differences using a numerical simulation of an airborne bistatic radar system.

2. *ADAPTIVE BISTATIC CLUTTER MITIGATION*

Bistatic ground clutter appears non-stationary in the range dimension due to non-proportionality between Doppler and spatial frequencies, even in the sidelooking receive case. This is brought about by the combination of projected transmitter and receiver velocity vectors, which determines the Doppler component [7-12, 14-17]. The degree of non-stationarity is highly dependent on the bistatic geometry and the range swath of interest. Non-stationarity degrades STAP performance through consequent covariance matrix estimation error.

The objective of STAP is to maximize output signal-to-interference-plus-noise ratio (SINR), thereby equivalently maximizing the probability of detection for a fixed false alarm rate (in the presence of Gaussian disturbance) [1]. The STAP combines *M* channel outputs and *N* pulses over *K* range bins; the corresponding output is $y_k = \hat{\mathbf{w}}_\mathbf{k}^H \mathbf{x}_\mathbf{k}$, where $\mathbf{x}_\mathbf{k} \in C^{NMx1}$ is the space-time observation vector and $\hat{\mathbf{w}}_\mathbf{k}$ is the adaptive weight vector. Given constant $\hat{\beta}$, covariance matrix estimate $\hat{\mathbf{R}}_\mathbf{k}$, and surrogate space-time steering vector $\mathbf{v}$, the adaptive weight vector follows as $\hat{\mathbf{w}}_\mathbf{k} = \hat{\beta}\hat{\mathbf{R}}_\mathbf{k}^{-1}\mathbf{v}$. An estimate of the unknown covariance matrix is given as

$$\hat{\mathbf{R}}_\mathbf{k} = \frac{1}{\tilde{K}} \sum_{m=1}^{\tilde{K}} \mathbf{x}_\mathbf{m}\mathbf{x}_\mathbf{m}^H \tag{1}$$

where the $\mathbf{x}_\mathbf{m}$ are known as training data [18]; in accord with [18], this estimator is maximum likelihood if the training data are Gaussian, independent and identically distributed (iid).

SINR loss factors conveniently characterize the impact of colored noise and errors in the adaptive process on output SINR [1-6]. Two useful SINR loss definitions used herein are:

$$\begin{aligned} L_{s,1} &= \frac{\text{output SINR for optimal filter}}{\text{signal-to-noise ratio}} = \text{clairvoyant loss;} \\ L_{s,2} &= \frac{\text{output SINR for adaptive filter}}{\text{output SINR for optimal filter}} = \text{adaptive loss.} \end{aligned} \tag{2}$$

Note that the calculation of $L_{s,1}$ requires the known covariance matrix.

When the training data are non-stationary (non-iid), as in the bistatic case, the adaptive filter converges to a response

Report Documentation Page

Form Approved
OMB No. 0704-0188

1. REPORT DATE	2. REPORT TYPE	3. DATES COVERED
01 MAY 2005	**N/A**	**-**

4. TITLE AND SUBTITLE	5a. CONTRACT NUMBER
Comparison of Bistatic Clutter Mitigation Algorithms For Varying Geometries	5b. GRANT NUMBER
	5c. PROGRAM ELEMENT NUMBER
6. AUTHOR(S)	5d. PROJECT NUMBER
	5e. TASK NUMBER
	5f. WORK UNIT NUMBER
7. PERFORMING ORGANIZATION NAME(S) AND ADDRESS(ES) **Georgia Tech Research Institute**	8. PERFORMING ORGANIZATION REPORT NUMBER
9. SPONSORING/MONITORING AGENCY NAME(S) AND ADDRESS(ES)	10. SPONSOR/MONITOR'S ACRONYM(S)
	11. SPONSOR/MONITOR'S REPORT NUMBER(S)

12. DISTRIBUTION/AVAILABILITY STATEMENT
Approved for public release, distribution unlimited

13. SUPPLEMENTARY NOTES
See also ADM002017. Proceedings of the 2005 IEEE International Radar Conference Record Held in Arlington, Virginia on May 9-12, 2005. U.S. Government or Federal Purpose Rights License., The original document contains color images.

14. ABSTRACT

15. SUBJECT TERMS

16. SECURITY CLASSIFICATION OF:			17. LIMITATION OF ABSTRACT	18. NUMBER OF PAGES	19a. NAME OF RESPONSIBLE PERSON
a. REPORT	b. ABSTRACT	c. THIS PAGE			
unclassified	**unclassified**	**unclassified**	**UU**	**6**	

representative of the average behavior of the secondary data set, rather than a response best suited to the particular range bin of interest. An increase in $L_{s,2}$ reflects this increased loss due to covariance estimation error.

2.1. *Bistatic Clutter Mitigation Techniques*

The class of adaptive bistatic clutter mitigation techniques generally fall into one of the following categories:

1. Methods attempting to limit the degree of range variability by selecting training data in proximity to the cell under test (accomplished by applying a reduced-rank or reduced-dimension STAP technique [1-6]);
2. Methods acknowledging the range non-stationary issue by allowing time evolution of the weight vector consistent with the presumed variation (e.g., linear variation over range) [9, 11, 12, 19]; and,
3. Methods either compensating or mapping training data to enforce alignment with a particular reference point [11, 13-17].

In this paper we focus on bistatic STAP methods falling within the third category and based on data warping. The algorithms having been previously reported include:

Doppler Warping (DW) [11, 13] – the processor accomplishes DW by temporally modulating the series of voltages recorded in each spatial channel to align the clutter Doppler to a reference.

Higher-Order Doppler Warping (HODW) [14] – this algorithm extends the DW concept to multiple receive angles, thereby aligning sections of the clutter ridge. The processor first transforms the data to beamspace, applies a different temporal modulation to each beam, and then inverse transforms to the space-time domain.

Angle-Doppler Compensation (ADC) [15] – this approach is similar in spirit to DW and HODW, but applies a range-varying space-time modulation to each range to align the peak clutter angle-Doppler response to a reference. Generally, ADC presumes perfectly characterized peak clutter response via precise knowledge of transmitter and receiver velocity vectors and array pointing directions.

Adaptive Angle-Doppler Compensation (A^2DC) [17] – this method extends the ADC approach by adaptively estimating the range-varying peak clutter angle-Doppler response. When the clutter environment is homogeneous and the platform velocity vectors, array normals, and steer directions are known, ADC and A^2DC yield virtually identical results.

2.2 *Influence of Bistatic Geometry*

Given the variation of Doppler with range and angle, the algorithms will be highly dependent on the scenario and geometry. We illustrate this point by considering the taxonomy of Figure 1, showing transmitter and mainbeam (blue triangle) and receiver position and mainbeam (red triangle), overlapped mainbeams, and platform direction indicated by the arrow located at either transmitter (Tx) or receiver (Rx). The chart also depicts the surface clutter Doppler (colors), iso-range contours (green ellipses) and the Doppler ambiguities (blue hyperbolas). This indicates the spatial variation of Doppler as seen by the receiver. The taxonomy covers four practical scenarios: (1) the pseudo-monostatic, sidelooking case, where gain patterns maximally overlap and Doppler variation over range for a given angle is slight; (2) the forward-looking adjunct, showing mild variation in gain pattern, but significant Doppler variation over range; (3) the hybrid scenario, with increased spatial gain variation and significant Doppler variation over range; and, (4) the near 90^o bistatic case, with severe spatial gain and Doppler variation.

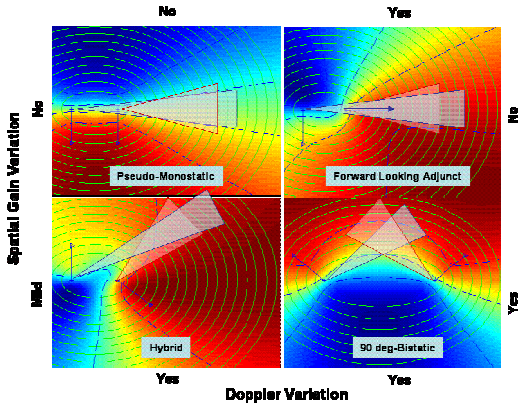

Fig. 1. Taxonomy of bistatic geometries affecting receiver Doppler

In the pseudo-monostatic case, data warping is unnecessary due to the lack of clutter non-stationarity. The processor employs localized training to cope with any heterogeneous conditions arising from varying clutter cultural features. Given the characteristics of the forward-looking adjunct, data alignment in the Doppler domain alone will prove adequate, a capability met by all four data warping strategies. Clutter non-stationarity increases in the hybrid scenario; under such circumstances, alignment in both angle and Doppler provides the potential for best performance. HODW's ability to align sections of the clutter ridge will also prove beneficial. Significant range variation in both angle and Doppler in the near 90^o bistatic scenario requires data warping in both domains to attain best performance; only ADC and A^2DC provide this capability.

3. *EVALUATION SCENARIO WITH HOMOGENEOUS CLUTTER*

Figure 2 depicts a bistatic geometry yielding significant clutter non-stationarity in both angle and Doppler. L_{TR} is the bistatic baseline; h_T and h_R indicate Tx and Rx platform altitudes; $\mathbf{v_T}$ and $\mathbf{v_R}$ represent Tx and Rx velocity vectors, where the *x*-component points due North, the *y*-axis aligns in the Westerly direction and the *z*-axis points away from the Earth's surface; and, $\mathbf{a_T}$ and $\mathbf{a_R}$ are the antenna normals,

each pointing in elevation at swath center denoted by *C*. This scenario is somewhat between hybrid and near-90° bistatic cases, though tending more towards the latter. As it represents a stressful scenario, it is a useful geometry for algorithm performance evaluation and suitable for the brief nature of this exposition.

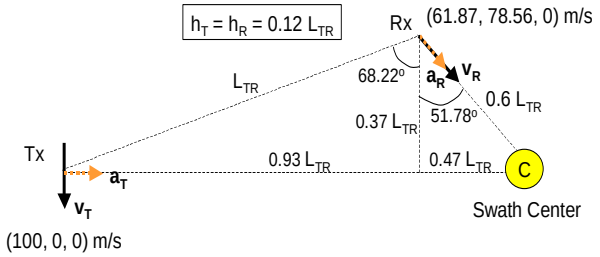

Fig. 2. Bistatic geometry yielding significant clutter non-stationarity

Table 1 provides salient parameters used in subsequent numerical simulation. Simulating the ground clutter response proceeds as follows. A representative, curved Earth's surface is pixelized to a fraction of a range-Doppler-angle resolution cell. We then calculate Tx and Rx gains and Doppler contributions at each pixel. Next, we generate the space-time response for each pixel commonly within Tx and Rx horizons, calculate the bistatic range sum, and then range bin the response. Finally, we sum all pixel responses corresponding to a particular range bin. The clutter complex envelope is Rayleigh-distributed, with reflectivity of –15 dB and sigma-0 following from the Bistatic Equivalence Theorem [20]. We further incorporate additive, white receiver noise with variance of one watt. Moreover, we calculate a *known* space-time covariance matrix for each range bin.

Table 1. Radar Parameters

Parameter	Value	Parameter	Value
Center Frequency	5.3 GHz	PRF	1,400 Hz
Uncompressed/ compressed pulse width	21.12 µs/ 0.33µs	Pulses (*N*)	16
Peak Transmit Power	10 kW	Array Configuration	Side-looking
Noise Figure	2.6 dB	Spatial Channels (*M*)	18
RF Losses	9.5 dB	Horizontal Element Spacing	0.58 wavelengths
Platform Velocity	100 m/s	Vertical Element Spacing	0.74 wavelengths

Figure 3 shows the precise spectral centers – clutter peak response in angle and Doppler – over bistatic range. From the simulation we retain 250 range bins – in large part due to memory storage used to record the space-time covariance matrix at each range – roughly focused on swath center; thus, range bin 125 is approximately the center of the scene shown in Figure 2. The dashed, horizontal line indicates the array normal, the dotted line shows peak azimuth measured from true North, and the solid line shows absolute Doppler (aliased in subsequent plots by the 1,400 Hz pulse repetition frequency (PRF)). The variation in both angle and Doppler over range is evident from this figure. As described in prior sections, this variation leads to covariance matrix estimation errors and degraded adaptive clutter mitigation.

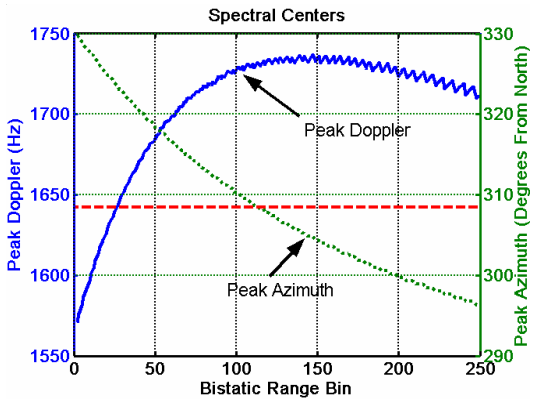

Fig. 3. Spectral centers

Figure 4 compares clairvoyant SINR loss for three steering angles calculated from array normal: 0°, -10°, and 10°. As expected, the strongest clutter for steer angle 0° corresponds to swath center, near bin 125, with Doppler from Figure 3 of 250-300 Hz (after accounting for Doppler aliasing). As the beam scans to negative azimuths, corresponding to a direction towards the transmitter, the peak response moves inwards in range and slightly downward in Doppler, results anticipated from Figures 2-3. Conversely, for positive steer angles, away from the transmitter, the peak response moves downward in range and upward in Doppler. This variation in peak response is further evidence of clutter non-stationarity.

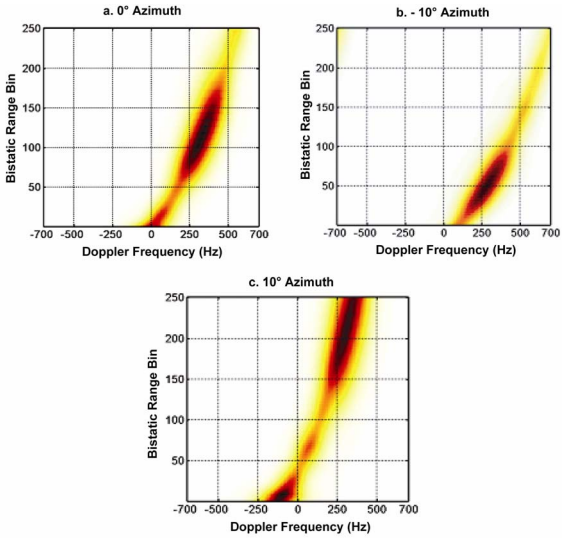

Fig. 4. Clairvoyant SINR loss for varying azimuth scan cases

4. *PERFORMANCE EVALUATION*

In this section we compare the performance of the aforementioned data warping techniques using the synthetic data whose characteristics are shown in Section 3. We consider performance for several implementations. All known covariance matrices undergo the various warping transformations to enable precise benchmarking. In our analysis, we consider the extended factored algorithm (EFA) of [21] with three temporal DoFs and the full complement of spatial DoFs, yielding fifty-four space-time DoFs.

Figure 5 shows the clairvoyant SINR loss for the broadside direction after applying DW, HODW, ADC, and A^{2}DC. DW, HODW and ADC all presume perfect *a priori* knowledge, whilst A^{2}DC derives all requisite information in situ. The HODW implementation warps eighteen beams – for an invertible transform – spaced six degrees apart from -54 to 48 degrees; since these beams are non-orthogonal, the HODW result does not default to the DW case. All data are warped to reference range bin 100. Figures 5a-5d capture the essence of the various compensation mechanisms. DW and HODW localize the clutter Doppler over range, but gain variation is evident. ADC and A^{2}DC localize both angle and Doppler responses. The similarity between ADC and A^{2}DC confirms the proper functioning of each algorithm. Due to this similarity, we subsequently only consider the A^{2}DC approach. Figure 6 and Figure 7 show adaptive SINR loss calculated at range bin 100 and the broadside direction. We also show the upper bound on performance (denoted "Ls_1" in the figure) for EFA and the joint-domain optimum (JDO) filter. In Figure 6, we train EFA over all 250 range bins, finding significant improvement for all data warping methods; performance for the unwarped case is abysmal. The similarity in performance among all three data warping methods is not surprising considering the cell under test and a substantial amount of training data reside in the peak clutter region; the losses due to undernulling of distributed clutter are mild. The slight "walk off" in clutter Doppler evident in Figure 5 is a likely result of the modest Doppler resolution; this effect leads to slight A^{2}DC losses to the right of the clutter null, but are likely correctable with increased temporal aperture. Figure 7 is contrasting: A^{2}DC performance is generally far superior to the other methods as a result of the limited training set. The peak characteristics of the training set show better match to the cell under test when applying A^{2}DC.

Factors leading to a reduced training set can include clutter heterogeneity (e.g., due to changing clutter types, shadowing, no return areas, etc.) and computational burden restricting data selection to a given region. A^{2}DC owes its performance enhancement to its ability to align the data in both angle and Doppler. Other implementations with varying training support, compensation points, or steer directions may be chosen to emphasize the notion that angle-Doppler warping provides an added degree of robustness.

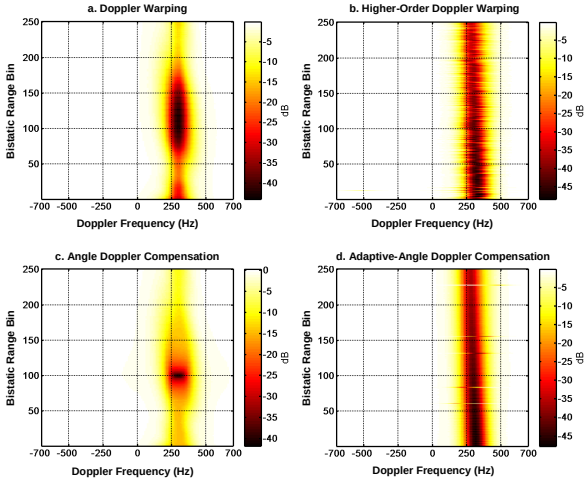

Fig. 5. Clairvoyant SINR loss post-data warping algorithms

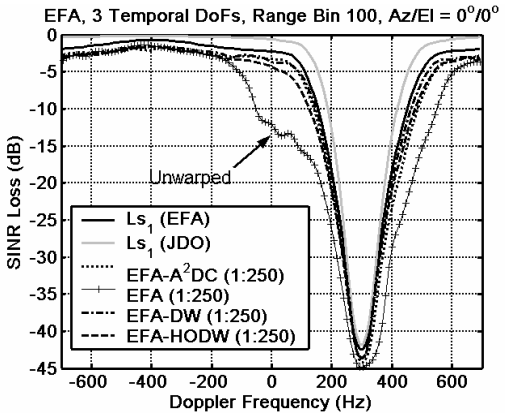

Fig. 6. Adaptive SINR loss comparing data warping schemes with training over all ranges (bins 1:250)

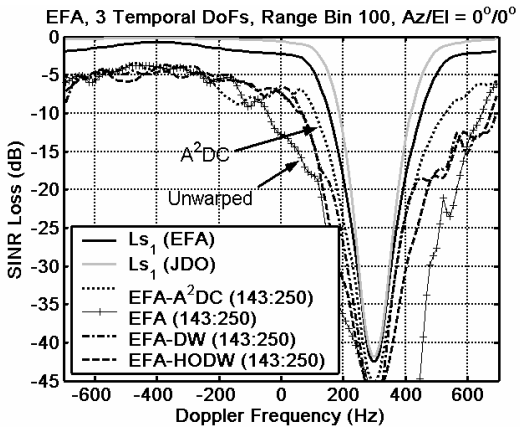

Fig. 7. Adaptive SINR loss comparing data warping methods with reduced training set (bins 143:250)

5. *PERFORMANCE IN HETEROGENEOUS CLUTTER*

Analysis in the prior section employed homogeneous terrain type to demonstrate performance improvement offered by the distinct capabilities of DW, HODW, ADC, and A^{2}DC data warping methods. It was further suggested that factors impacting the uniformity of the peak clutter response over range, such as clutter heterogeneity, affect algorithm performance. This section briefly considers site-specific clutter effects and their potential consequences for bistatic STAP techniques.

We modeled two scenarios based upon the geometry in Figure 2 and radar system information in Table 1 using RLSTAP, a radar system modeling and simulation tool developed by the Air Force Research Laboratory (AFRL). The first scenario corresponds to homogeneous terrain type, with clutter reflectivity governed by the constant gamma model [20], whilst the second scenario employs a site-specific clutter model corresponding to Northwestern New York State, USA, where a rich variety of terrain types are present. The site-specific terrain resolution is approximately 90 meters by 90 meters and is available for public download from the United States Geological Survey's (USGS) web site.

Figure 8 shows a plot of the product of transmit gain, receive gain, and "normalized scatterer" response (which takes into account terrain cell area, sigma-0, and range effects) for one of the eighteen receive channels. Each single receive channel has a very broad antenna pattern in azimuth. The transmit system is denoted by a cluster of red icons, the receive system by a cluster of green icons, and the aim point of transmit and receive beams by a cluster of purple icons. High intensity is denoted by lighter colors (with white being the most intense) and low intensity by darker hues. Figure 8 highlights the broadened two-way gain illuminating the Earth's surface and leading to severe clutter conditions.

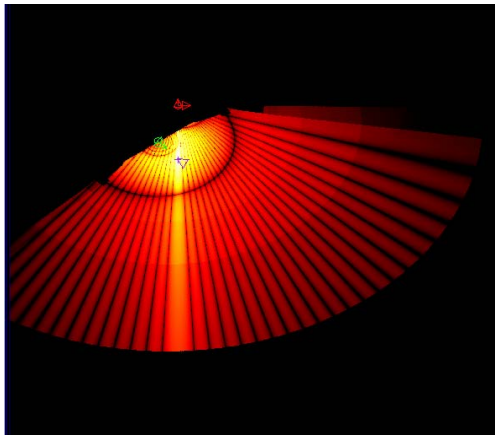

Fig. 8. Normalized reflected power for the homogeneous clutter case generated using RLSTAP

Figure 9 shows the reflected power for the case of site-specific terrain. In contrast to Figure 8, the non-uniform variation in reflected power is evident. This variation affects the *a priori* calculation of peak clutter response and utility of one-dimensional warping. Specifically, the peak clutter response must either incorporate site-specific information, or estimate the peak *in situ*, as in the case of A^{2}DC.

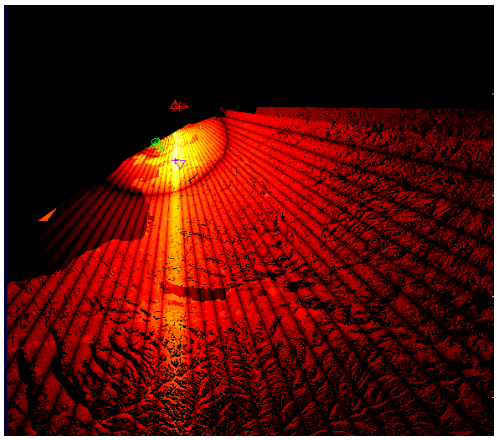

Fig. 9. Normalized reflected power for site-specific clutter scenario – Northwestern New York State – generated using RLSTAP

Next, we duplicate the previous SINR loss analysis of Section 4 using the RLSTAP-generated data consisting of the datacube of complex voltages and known covariance matrices at select ranges. As in the prior section, we apply the EFA STAP method and consider performance with and without data warping. We only consider the A^{2}DC warping method, as it showed best performance in the prior section, requires no a priori knowledge, and can track variation in peak clutter response. Figure 10 and Figure 11 are the site-specific counterparts to Figure 6 and Figure 7. Observe the closely matching clutter nulls, confirming the veracity of the two different simulations (based on Georgia Tech models in Section 4 and RLSTAP in this section). From both Figure 10 and Figure 11 we again find tremendous improvement resulting from application of the A^{2}DC warping method. Overall, however, the loss levels are greater than in Figure 6 and Figure 7. We attribute this additional loss to the impact of clutter heterogeneity, which is not entirely compensated by the data warping method.

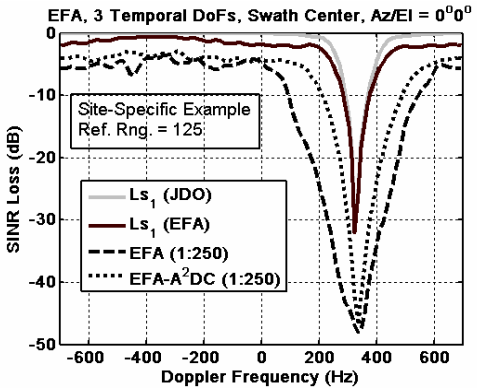

Fig. 10. Adaptive SINR loss for site-specific case, training over all range

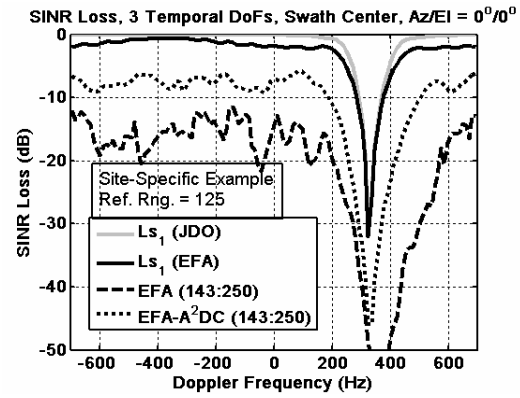

Fig. 11. Adaptive SINR loss, site-specific case, reduced training set

6. *SUMMARY*

This paper considered the performance of the class of data warping-based bistatic STAP techniques as a function of sensor geometry. Specific contributions made herein include:

- Development of a taxonomy of bistatic geometry and identification of consequences for data warping algorithms;
- Rigorous benchmarking of data warping methods for a specific scenario involving clutter non-stationarity in both angle and Doppler; and,
- Consideration of the impact of site-specific clutter on bistatic STAP performance.

Our findings suggest that all data warping methods provide substantial enhancement over traditional (unwarped) STAP implementation. Those methods warping the data in both angle and Doppler – *viz.*, ADC and A^2DC – lead to the most homogeneous training set, and consequently the potential for more robust adaptive filter implementation.

Future work should consider the impact of site-specific clutter in further detail, as well as other factors affecting algorithm robustness (e.g., the required accuracy of *a priori* knowledge, factors impacting estimation accuracy, etc.).

ACKNOWLEDGMENT

This work was supported by the US Air Force under Contract Number F30602-02-C-0094.

REFERENCES

1. L. E. Brennan and I. S. Reed, "Theory of adaptive radar," *IEEE Transactions AES*, Vol. 9, No. 2, March 1973, pp. 237-252.
2. J. R. Guerci, *Space-Time Adaptive Processing for Radar*, Artech House, Norwood, MA, 2003.
3. R. Klemm, *Space-Time Adaptive Processing: Principles and Applications*, IEE Radar, Sonar, Navigation and Avionics 9, IEE Press, 1998.
4. R. Klemm, *Principles of Space-Time Adaptive Processing*, IEE Radar, Sonar, Navigation and Avionics 12, IEE Press, 2002.
5. J. Ward, "Space-time adaptive processing for airborne radar," Lincoln Laboratory Tech. Report, ESC-TR-94-109, December 1994.
6. W. L. Melvin, "A STAP overview," *IEEE AES Systems Magazine – Special Tutorials Issue*, Vol. 19, No. 1, January 2004, pp. 19-35.
7. R. Klemm, "Comparison between monostatic and bistatic antenna configurations for STAP," *IEEE Trans. AES*, Vol. 36, No. 2, pp. 596-608, April 2000.
8. P. G. Tomlinson, "Modeling and analysis of monostatic/bistatic space-time adaptive processing for airborne and space-based radar," in *Proc. IEEE 1999 National Radar Conf.*, Boston, MA, pp. 102-107, April 1999.
9. W. L. Melvin, M. J. Callahan, M. C. Wicks, "Adaptive clutter cancellation in bistatic radar," in *Proc. 34th Asilomar Conf*., Pacific Grove, CA, pp. 1125-1130, Oct 2000.
10. B. Himed, J. H. Michels, and Y. Zhang, "Bistatic STAP performance analysis in radar applications," in *Proc. 2001 IEEE Radar Conf*., Atlanta, GA, May 2001, pp. 198-203.
11. S. M. Kogon and M. A. Zatman, "Bistatic STAP for airborne radar systems," in *Proc. IEEE SAM 2000*, Lexington, MA, March 2000.
12. W. L. Melvin, M. J. Callahan, and M. C. Wicks, "Bistatic STAP: application to airborne radar," in *Proc. 2002 IEEE Radar Conf*., Long Beach, CA, 22-25 April 2002, ISBN: 0-7803-7358-8.
13. G. Borsari, "Mitigating effects on STAP processing caused by an inclined array," in *Proc. 1998 IEEE Radar Conf*., Dallas, Tx, pp. 135-140, May 1998.
14. F. Pearson and G. Borsari, "Simulation and analysis of adaptive interference suppression for bistatic surveillance radars," in *Proc. 2001 ASAP Symp*., Lexington, MA, 13 March 2001.
15. B. Himed, Y. Zhang, and A. Hajjari, "STAP with angle-Doppler compensation for bistatic airborne radars," in *Proc. 2002 IEEE Radar Conf*., Long Beach, CA, 22-25 April 2002, ISBN: 0-7803-7358-8.
16. F. D. Lapierre, J. G. Verly, and M. Van Droogenbroeck, "New solutions to the problem of range dependence in bistatic STAP radars," in *Proc. 2003 IEEE Radar Conf*., Huntsville, AL, 5-8 May 2003, pp. 452-459.
17. W. L. Melvin, B. Himed, and M. E. Davis, "Doubly-adaptive bistatic clutter filtering," in *Proc. 2003 IEEE Radar Conf*., Huntsville, AL, 5-8 May 2003, pp. 171-178.
18. I. S. Reed, J. D. Mallett, and L. E. Brennan, "Rapid convergence rate in adaptive arrays," *IEEE Trans. AES*, Vol. 10, No. 6, November 1974, pp. 853-863.
19. S. D. Hayward, "Adaptive beamforming for rapidly moving arrays," in *Proc. CIE Int'l Conf. of Radar (IEEE Press)*, Beijing, China, 8-10 October 1996, pp. 480-483.
20. N. J. Willis, *Bistatic Radar*, Technology Service Corporation, Silver Spring, MD, 1995.
21. R. C. DiPietro, "Extended factored space-time processing for airborne radar," in *Proc. 26th Asilomar Conf*., Pacific Grove, CA, Oct. 1992, pp. 425-430.